

New Developments and Applications of the MP2RAGE Sequence - Focusing the Contrast and High Spatial Resolution R_1 Mapping

José P. Marques^{1,2*}, Rolf Gruetter^{1,2,3}

1 Department of Radiology, University of Lausanne, Lausanne, Switzerland, **2** Laboratory for Functional and Metabolic Imaging, Ecole Polytechnique Fédérale de Lausanne, Lausanne, Switzerland, **3** Department of Radiology, University of Geneva, Geneva, Switzerland

Abstract

MR structural T_1 -weighted imaging using high field systems ($>3T$) is severely hampered by the existing large transmit field inhomogeneities. New sequences have been developed to better cope with such nuisances. In this work we show the potential of a recently proposed sequence, the MP2RAGE, to obtain improved grey white matter contrast with respect to conventional T_1 -w protocols, allowing for a better visualization of thalamic nuclei and different white matter bundles in the brain stem. Furthermore, the possibility to obtain high spatial resolution (0.65 mm isotropic) R_1 maps fully independent of the transmit field inhomogeneities in clinical acceptable time is demonstrated. In this high resolution R_1 maps it was possible to clearly observe varying properties of cortical grey matter throughout the cortex and observe different hippocampus fields with variations of intensity that correlate with known myelin concentration variations.

Citation: Marques JP, Gruetter R (2013) New Developments and Applications of the MP2RAGE Sequence - Focusing the Contrast and High Spatial Resolution R_1 Mapping. PLoS ONE 8(7): e69294. doi:10.1371/journal.pone.0069294

Editor: Essa Yacoub, University of Minnesota, United States of America

Received: December 12, 2012; **Accepted:** June 7, 2013; **Published:** July 16, 2013

Copyright: © 2013 Marques, Gruetter. This is an open-access article distributed under the terms of the Creative Commons Attribution License, which permits unrestricted use, distribution, and reproduction in any medium, provided the original author and source are credited.

Funding: This work was supported by Centre d'Imagerie BioMédicale (CIBM) of the UNIL, UNIGE, HUG, CHUV, EPFL, and the Leenaards and Jeantet Foundations. The funders had no role in study design, data collection and analysis, decision to publish, or preparation of the manuscript.

Competing Interests: The authors have declared that no competing interests exist.

* E-mail: jose.marques@epfl.ch

Introduction

The promise of ultra high fields systems to provide higher spatial resolution structural images due to their higher signal to noise ratio (SNR) has been hampered by the increase in transmit magnetic field inhomogeneities and the high specific absorption rate (SAR) that come associated with the decrease of the wavelength and increased frequency of the RF pulses that are used to excite the proton spins [1]. SAR limitations have made gradient echo based sequences to be the main workhorse of structural imaging at high fields, delivering either T_2^* -weighted imaging [2], phase imaging [3] and T_1 -weighted imaging. The MP2RAGE sequence has been recently introduced as a means to obtain bias field free T_1 -weighted images and jointly estimating T_1 maps at ultrahigh field [4,5]. In the original work, the sequence parameter optimization was developed to obtain the conventional range of contrast used in T_1 -weighted imaging (covering the T_1 range from white matter to cerebro spinal fluid) with the protocols being defined in order to achieve reliable T_1 maps when the typical clinical whole brain isotropic resolution of approximately 1 mm was desired. Although such a large range of T_1 range and conservative resolution is desirable for normal brain imaging and segmentation applications, it is not ideal when looking at detailed visualization of deep gray matter structures [6] or fine variations in cortical relaxation properties throughout the brain [7].

Visualization of deep gray matter structures such as the different thalamus nuclei, striatum, external and internal globus pallidus (GPe/GPi), red nucleus (RN) and substantia nigra (SN) can be of great importance in applications such as deep brain stimulation

(DBS) used in the treatment of involuntary movement disorders, in Parkinson's disease or dystonia [8,9]. Attempts to automatically segment the thalamus nuclei using structural imaging have to date had some success [10,11], but only limited correlation was found with thalamic segmentation using either diffusion weighted imaging [12] or histology. Due to the low levels of contrast between the basal ganglia and surrounding structures in T_1 -w images, a number of approaches using other contrast have been explored [10,13–15]. Among these, a recent studies have proposed a modification of the standard MPRAGE sequence parameters to yield a better visualisation of basal ganglia structures [16] and subthalamic nuclei [17] by using a shorter inversion time than the usually used at the respective field strengths (in which the CSF signal is nulled). Recently in a 3T study, the MP2RAGE was modified [18] in order to provide two T_1 -weighted images, one with the conventional MPRAGE contrast (with CSF nulling) and one with a short TI where the WM signal is suppressed.

Despite the optimization of the MP2RAGE sequence parameters [5] performed in order to reduce B_1^+ dependence of those images (at a cost of a reduction of the contrast obtainable), the resulting T_1 -maps still suffer from some residual transmit field bias. Furthermore, the temptation to increase the resolution (by increasing the number of low flip angle excitations per TR) and the need to keep the total acquisition time low (by reducing the TR of the MP2RAGE), increase the sensitivity of the MP2RAGE T_1 estimation to B_1^+ inhomogeneities. Recently, some attention has been drawn to the correlation between the observed cortical T_1 values and known distributions of myelination [7,19,20]. For these correlations to be further evaluated at such high resolution and

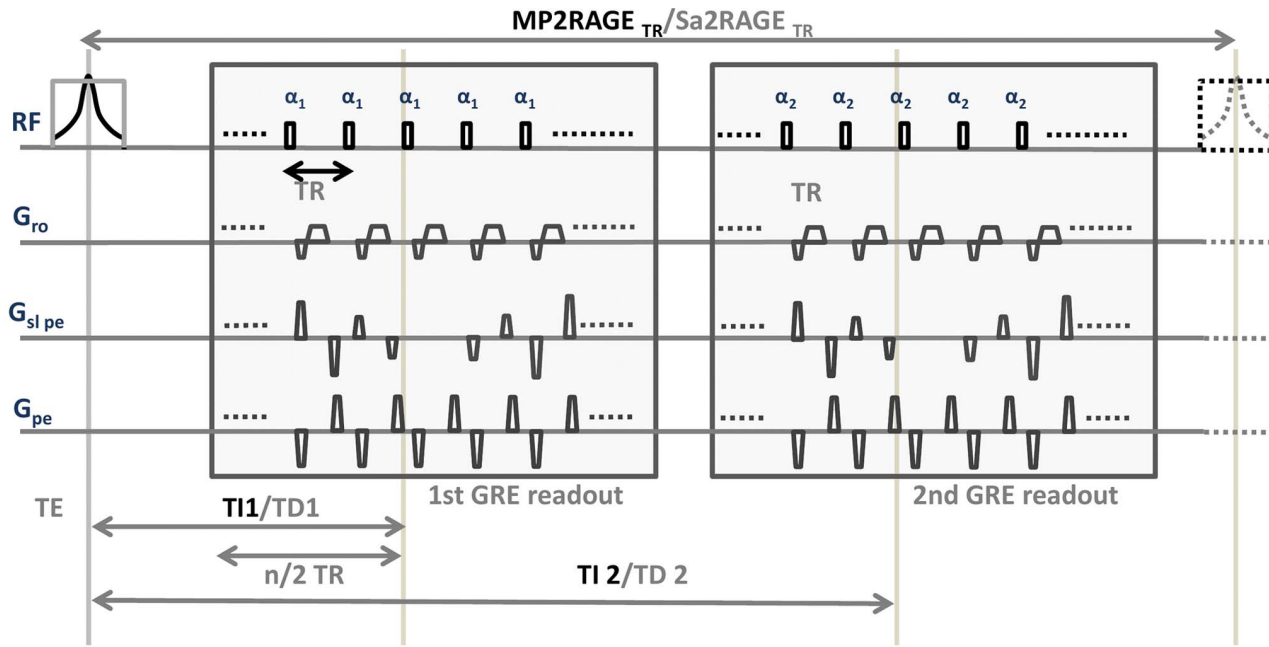


Figure 1. Diagram of the MP2RAGE and Sa2RAGE sequences. Inversion (Delay) times T_{I1} and T_{I2} (T_{D1} and T_{D2}) are defined as the time from the middle of the inversion (saturation) pulse to the excitation corresponding to the center k-space line in the phase encoding in the slab selection direction. $MP2RAGE_{TR}$ is the time between two successive inversion pulses and TR is the time between successive excitation pulses in the GRE kernel which is composed of n excitations. Features specifically associated with the MP2RAGE and Sa2RAGE are shown in black and light grey respectively (the adiabatic inversion and the saturation pulse). The gradient echo excitation pulses used for both the SA2RAGE and MP2RAGE were non-frequency selective.

doi:10.1371/journal.pone.0069294.g001

through such a large brain extent, it is imperative to obtain high resolution, robust and fully bias free T_1 values. Often, the effect of T_1 relaxation and B_1^+ inhomogeneity on signal are intertwined and most techniques proposed to measure T_1 effectively measure these T_1 and B_1^+ simultaneously [21–26]. This can be done either within one single acquisition, which impacts on the SNR efficiency of the method, or using separate acquisitions.

In this work, we explore different potential high field applications of the MP2RAGE sequence: (i) improved contrast between white matter and grey matter tissues allowing clear visualization of sub-thalamic nuclei and other deep grey matter structures; (ii) high resolution T_1 maps with optimum contrast to noise ratio in which the effects of significant B_1 field inhomogeneities are taken into account by combining the MP2RAGE sequence with the Sa2RAGE sequence [27] and study R_1 variations throughout the cortex and in different white matter bundles.

Theory and Methods

The MP2RAGE sequence can be described as an inversion recovery sequence in which two gradient echo images are acquired during the recovery period with different inversion times ($GRE_{T_{I1}}$ and $GRE_{T_{I2}}$). The MP2RAGE image is a synthetic image obtained from a combination of the two acquisitions:

$$MP2RAGE = \frac{GRE_{T_{I1}} GRE_{T_{I2}}^*}{GRE_{T_{I1}}^2 + GRE_{T_{I2}}^2} \quad (1)$$

both images are taken as complex images and the asterisk stands for the complex conjugate.

The Sa2RAGE sequence is a saturation recovery sequence in which two images are acquired before ($GRE_{T_{D2}}$) and after ($GRE_{T_{D1}}$) a saturation pulse (see Figure 1 for a more complete description). A full Bloch equation simulation of the sequence permits the mapping of the transmit field B_1 . It was shown [27] that this technique could provide B_1 maps at 7T with small errors even when assuming a common T_1 value for the whole brain.

Simulations

The optimum sequence parameters for the different applications were studied via simulations. The predicted MP2RAGE signal amplitudes for several tissues were numerically calculated after solving the Bloch Equations as in reference [5].

When studying the (i) optimum contrast between white matter WM, thalamus and Gray Matter the following parameters were considered fixed: number of excitations per GRE module was set to 160 (full k-space coverage) or 120 (partial fourier k-space coverage); The contrast at 7 Tesla was evaluated for 5 different T_1 values, ranging from 1.1 ($\sim T_{1WM}$) to 1.9s ($\sim T_{1GM}$) [5]. The range of T_1 values chosen should cover the different T_1 values in the thalamus and the choice of the number of excitations was done to allow a 1mm isotropic resolution with full brain coverage in sagittal orientation.

When studying the (ii) optimum contrast achievable at high resolution (0.65 mm isotropic): Number of excitations per GRE module was set to 192 (partial fourier k-space coverage 6/8–256 partitions); 5 T_1 values equally spaced ranging from 1.1 ($\sim T_{1WM}$) to 4 s ($\sim T_{1CSF}$). The range of T_1 values was chosen in order to include all brain tissues and CSF, while the choice of the number of excitations was done to achieve a 0.65 mm isotropic resolution with full brain coverage in sagittal orientation.

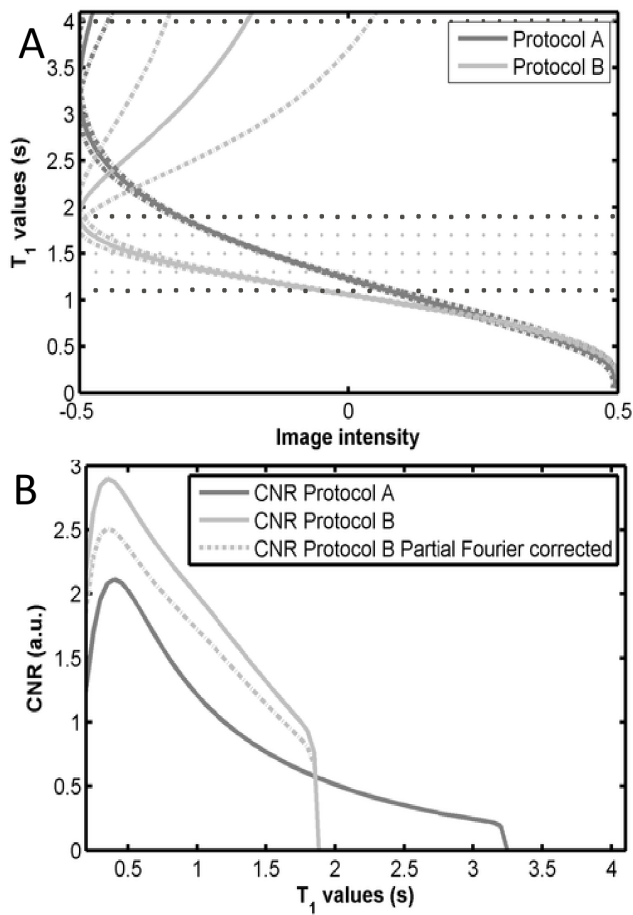


Figure 2. Plots of the theoretical relationship between T_1 values and MP2RAGE intensity. (a) MP2RAGE as a function of T_1 for the parameters that optimize contrast over all values of T_1 present in the brain (dark grey line) and the parameters that optimize contrast for T_1 values between those of WM and GM (light grey). The dashed lines represent the variation in intensities when the effective B_1^+ is $\pm 40\%$ of the nominal value while dark dotted lines show the T_1 values for which Protocol A was optimised and light dotted lines show the T_1 values for which Protocol B was optimised. (b) Plot of the contrast to noise ratio between successive T_1 values ($\delta T_1 = 0.05$ s) for the different protocols as a function of T_1 . The dashed line shows the corrected CNR when the effect of the Partial Fourier in protocol B is taken into account. doi:10.1371/journal.pone.0069294.g002

In both cases, the following parameters were varied in order to compute the optimum protocols: $MP2RAGE_{TR}$, TI_1 and TI_2 , α_1 and α_2 (see Figure 1 for a complete overview of the sequence and the meaning of the different parameters).

Contrast to noise by unit of time between two tissues (i and j) with successive values of T_1 was defined as:

$$\frac{S_i - S_j}{\sqrt{\sigma_{S_i}^2 + \sigma_{S_j}^2}} \frac{1}{\sqrt{TR}} \quad (2)$$

Where S_i is the calculated MP2RAGE signal [5] of tissue i, and its noise, σ_{S_i} , was estimated by error propagation of the MP2RAGE signal equation. The contrast to noise ratio between the successive T_1 values was integrated in order to obtain the sequence CNR for the desired application.

Sequence parameters were chosen from the simulations in order to optimize the CNR for the desired T_1 range and for the desired resolution. A ground truth T_1 mapping protocol was designed to evaluate the accuracy of the T_1 correction methodology (experiment ii). The ground truth protocol consisted of an MP2RAGE acquisition with a reduced number of rf pulses during the recovery process (hence, to keep the FOV the same, a lower resolution was used) and reduced flip angle amplitude for both echo trains (ensuring the low B_1^+ inhomogeneity sensitivity). In this protocol, the maximum achievable CNR was penalized in order to have a bias in the T_1 mapping under 5% for all tissues in the brain when in the presence of B_1 field deviations as large as $\pm 40\%$ of the nominal value.

Experimental Protocol

Data were collected at a short-bore 7T MR system (Siemens, Germany) equipped with a head-gradient insert and a 32-channel head coil (Nova Medical Inc) for reception. All subjects provided written informed consent and the study was approved by the local ethics committee (Commission cantonale VD d'éthique de la recherche sur l'être humain).

(i) MP2RAGE data from 3 subjects (age = 24 ± 4 years) were acquired using the following sequence parameters:

- a) $MP2RAGE_{TR}/TI_1/TI_2 = 6/0.8/2.5$ s and $\alpha_1/\alpha_2 = 4/5$ degrees (Protocol A);
- b) optimized for the white to grey matter T_1 range $MP2RAGE_{TR}/TI_1/TI_2 = 6/0.7/1.6$ s and $\alpha_1/\alpha_2 = 7/7$ degrees (Protocol B).

Both acquisitions were performed using $iPAT_{PE} = 2$ and 6/8 k-space coverage on the slice encoding direction, acquisition time of 10 mins. The matrix size and resolution were of $256 \times 200 \times 176$ and 0.85 mm isotropic respectively, while the BW was of 240 Hz per pixel.

(ii) Data from 4 subjects (age = 28 ± 4 years) were acquired using the following sequences:

- a) MP2RAGE sequence: $MP2RAGE_{TR}/TI_1/TI_2 = 6/0.8/2.7$ s, $\alpha_1/\alpha_2 = 7/5$ degrees (protocol A - high CNR), matrix size and resolution were of $320 \times 320 \times 256$ and 0.65 mm isotropic, $T_{acq} = 10$ min, $iPAT_{PE} = 3$ and 6/8 k-space;
- b) MP2RAGE sequence: $MP2RAGE_{TR}/TI_1/TI_2 = 6/0.8/2.7$ s, either $\alpha_1/\alpha_2 = 3/4$ (protocol B - reduced B_1^+ sensitivity), BW = 300 Hz per pixel, matrix size and resolution were of $192 \times 192 \times 160$ and 1 mm isotropic, $T_{acq} = 10$ min.26 secs;
- c) Sa2RAGE sequence: $Sa2RAGE_{TR}/TD_1/TD_2 = 2.4/0.058/1.8$ s, $\alpha_1/\alpha_2 = 4/11$ degrees, $TR_{GRE} = 3$ ms, BW = 1950 Hz per pixel, matrix size and resolution were of $128 \times 120 \times 64$ and $2 \times 2 \times 2.5$ mm³ resolution, $iPAT_{PE1} = 2$ and 6/8 partial Fourier sampling were used in the phase encoding direction and slice encoding direction respectively. $T_{acq} = 2.30$ min (see Fig. 1 for more details regarding the sequence);

The whole scan was repeated for one of the subjects with dielectric pads [28,29] positioned on one side of the head to guarantee that a different B_1^+ pattern would be present.

Processing Protocol (i)

When performing the optimization of the MP2RAGE sequence parameters to enhance the contrast for a limited range of T_1 values (from 1.1 to 1.9 s), it is possible to observe (see Fig. 2a), that the relationship between T_1 and MP2RAGE signal intensity is no longer monotonous. The CSF intensity appears aliased to intensity

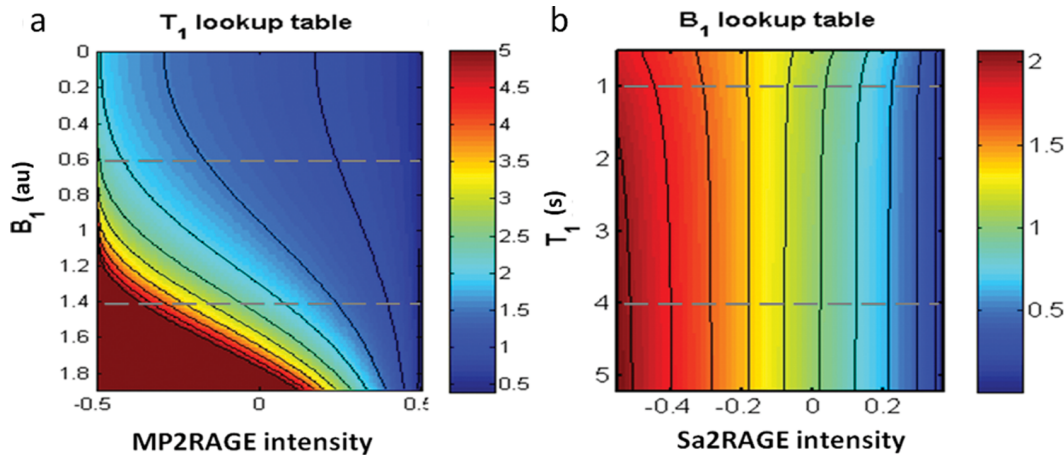


Figure 3. Lookup tables used to compute: (a) the R_1 ($1/T_1$) maps for the MP2RAGE sequence with $MP2RAGE_{TR}/T_1/T_2 = 6/0.8/2.7$ s, $\alpha_1/\alpha_2 = 7/5$ (protocol ii-A), (b) the B_1 maps for the Sa2RAGE sequence with $Sa2RAGE_{TR}/TD_1/TD_2 = 2.4/0.058/1.8$ s, $\alpha_1/\alpha_2 = 4/11$. Grey dashed lines define the typical range of B_1 and T_1 observed in the human brain at 7T ($\pm 40\%$ of the nominal B_1 value). doi:10.1371/journal.pone.0069294.g003

values close to that of WM. Using the Bloch simulations it is possible to recover the full range by using information from a complex ratio between the second and first inversion time images [4], which is monotonic as a function of T_1 . Although this new image, $MP2RAGE_{WMGMFullRange}$, has exactly the same contrast properties as the $MP2RAGE_{WMGM}$, the fact that CSF appears dark makes the interpretation of the images easier.

Using the sequence parameters suggested to enhance subthalamic contrast, the intensity of WM and of CSF are close to zero in the first and second inversion contrasts respectively (note that in Fig. 2a both have an MP2RAGE intensity of ~ 0). This is a similar scenario to that observed in the FLAWS sequence, where this feature was used to create Double Inversion Recovery like images [18]. Because of the specificities of the receive and transmit field inhomogeneities observed at 7T, the MP2RAGE MIP (minimum intensity projection) images were computed as:

$$MIP = \frac{\min(GRE_{T1}, GRE_{T2})}{\text{abs}(GRE_{T1}) + \text{abs}(GRE_{T2})} \quad (3)$$

To obtain a quantitative evaluation of the contrast obtained using the different sequence parameters, regions of interest were defined on the images of protocol A ($MP2RAGE$) and protocol B ($MP2RAGE_{WMGM}$) using MRIcro [30] and their intersection was used to evaluate the mean and standard deviation of the signal. The contrast to noise ratio between different structures was quantified as in Eq. 2.

Processing Protocol (ii)

The Sa2RAGE image (ii-c) and the low resolution MP2RAGE image (ii-b) were co-registered to the high resolution MP2RAGE image using FLIRT (www.fmrib.ox.ac.uk/fsl). The co-registration was performed using the images with higher signal intensity and lower contrast (2nd contrast from the Sa2RAGE and MP2RAGE sequences) and the spatial transforms were subsequently applied to the synthetic images. Re-sampling was performed using a sinc interpolation.

In the original MP2RAGE T_1 map calculation [5], lookup tables were used to, assuming the transmit field was equal throughout the whole image, relate the MP2RAGE intensity to a

T_1 value. A similar process was used to calculate B_1^+ maps using the Sa2RAGE sequence [27], where an average T_1 value was assumed to be valid throughout the brain and was demonstrated to have a reduced impact in terms of the robustness of the calculated B_1^+ maps. In this work, 2D lookup tables containing the T_1 values associated to certain MP2RAGE signal and B_1^+ value (see Fig. 3a for the MP2RAGE protocol A) and the B_1 values associated to certain Sa2RAGE signal and T_1 value (see Fig. 3b referring to the Sa2RAGE protocol) were computed. A two dimensional interpolation was iteratively performed for each pixel using the two lookup tables. Given the higher independence of B_1^+ estimation on the T_1 values (see Fig. 3b), the B_1^+ was first calculated for each pixel assuming constant T_1 throughout the brain (1.5 s). These B_1^+ values were then used to estimate the T_1 values via a 2D interpolation of the MP2RAGE lookup table (Fig. 3a). The process was repeated using the newly updated T_1 estimates for each voxel. At the third iteration, the variations in both B_1^+ and T_1 were found to be under 10^{-3} .

To evaluate the effectiveness of the B_1 correction, the corrected R_1 maps ($1/T_1$) acquired with the high-resolution (and high CNR) protocol (ii-A) were compared with the low resolution (and low B_1 -sensitivity) protocol (ii-B) in terms of general similarity between the distribution of R_1 values throughout white and grey matter.

The quality of the anatomical information present in high resolution R_1 maps was evaluated by observing the contrast and anatomical detail observed in structures such as the hippocampus. The individual R_1 maps were processed with freesurfer (<http://surfer.nmr.mgh.harvard.edu/>) to create cortical surface models [31]. Five equally spaced surfaces were generated in between the white matter and pial surfaces in order to study cyto-architectonic cortical variations in the mid layer throughout the brain. A 2 mm smoothing along the surface was applied and the R_1 surface maps were then plotted using MATLAB (The MathWorks Inc.).

Results

Simulations showed that the parameters that optimise T_1 contrast between WM and GM are obtained by reducing the spacing between the two different inversion times (see experimental Protocol i-b). Figure 2a shows the lookup tables of the MP2RAGE signal intensity as a function of the T_1 values for the protocols with $TR = 6$ secs optimized for full T_1 range contrast or

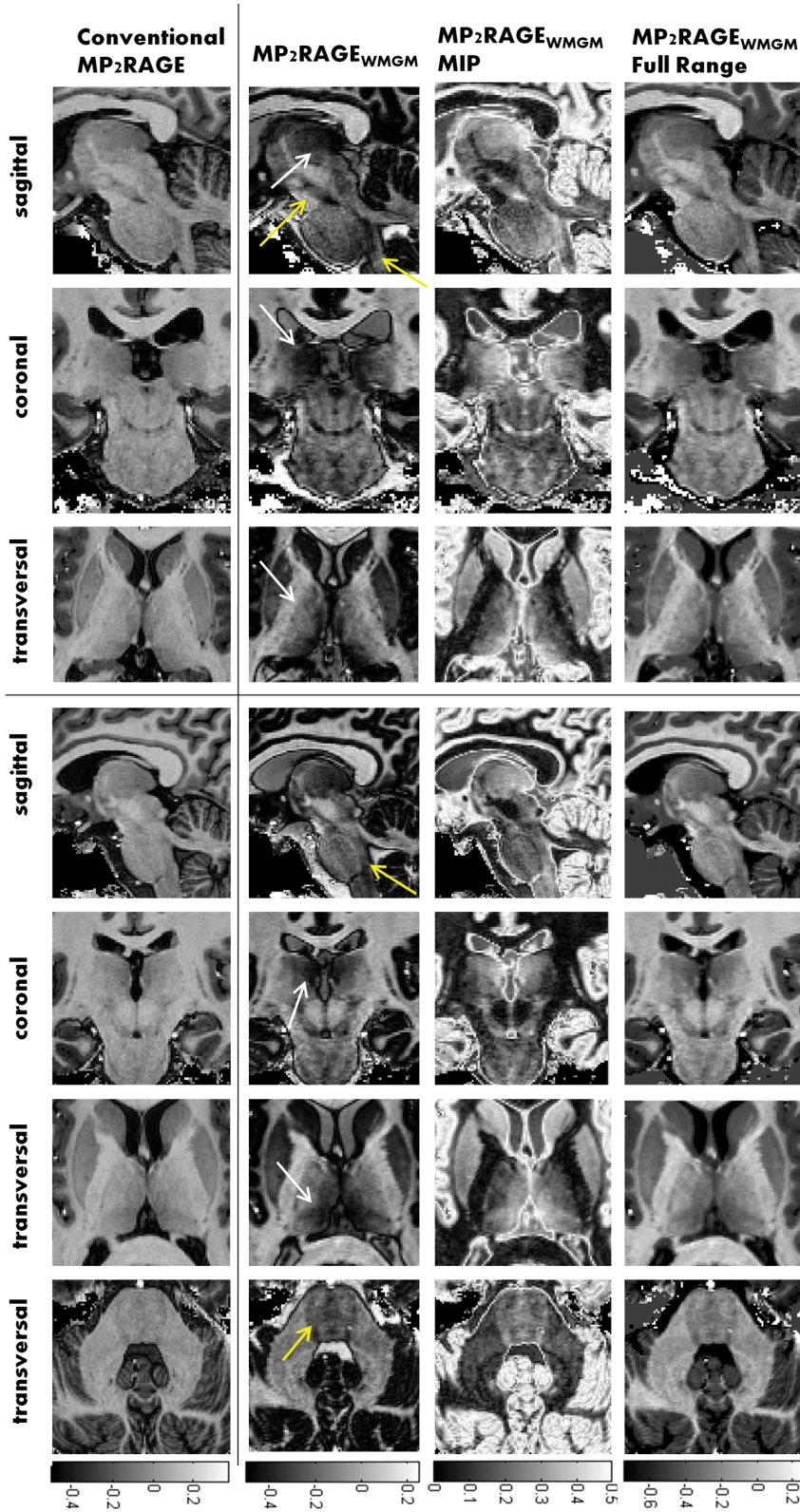


Figure 4. Panels with representative data from the two different subjects (Subject 1 - top three rows, Subject 2 -bottom 4 rows). The different columns show:(1st column) conventional MP2RAGE; (2nd column) MP2RAGE optimized for WM GM contrast;(3rd column) MP2RAGE MIP images and (4th column) full range MP2RAGE_{WMGM}images. Yellow arrows point regions where the increased WM T1 sensitivity of the new protocol allows the visualization of brain stem and pons sub-structures, while white arrows show the delineation the medio-dorsal, ventral lateral and pulvinar nuclei of the thalamus.

doi:10.1371/journal.pone.0069294.g004

Table 1. Table showing the mean contrast to noise ratio between different brain regions with T_1 values in between that of cerebral white matter and cortical grey matter.

Contrast to Noise Ratio	MP2RAGE	MP2RAGE _{WMGM}	MIP	MP2RAGE _{FULLRANGE}
Medial Thalamus ($1.4 \pm 0.1 \text{ cm}^3$) vs Outer thalamus ($3.2 \pm 1.5 \text{ cm}^3$)	2.5 ± 0.2	3.0 ± 0.5	2.8 ± 0.4	3.0 ± 0.5
Outer Thalamus ($3.2 \pm 1.5 \text{ cm}^3$) vs White Matter ($163 \pm 73 \text{ cm}^3$)	1.9 ± 0.5	2.5 ± 0.7	2.6 ± 0.7	2.5 ± 0.7
Caudate ($2.1 \pm 0.6 \text{ cm}^3$) vs Putamen ($1.7 \pm 0.1 \text{ cm}^3$)	0.5 ± 0.2	0.7 ± 0.4	0.7 ± 0.4	0.7 ± 0.4
Brain Stem ($3.3 \pm 0.7 \text{ cm}^3$) vs Cerebellum white matter ($3.6 \pm 1.5 \text{ cm}^3$)	1.5 ± 0.4	2.4 ± 0.2	2.3 ± 0.2	2.4 ± 0.2

The contrast to noise ratio was evaluated on the same regions of interest for the 2 different sequences (and 4 different contrasts). The mean volume of each region of interest is shown in the left column in parenthesis in cm^3 .

doi:10.1371/journal.pone.0069294.t001

WM-GM contrast (see Fig. 2a). Using partial k-space sampling in the slice encoding direction it was possible to reduce the number of excitations per GRE block and the sensitivity of the resulting image to transmit B_1 field inhomogeneities (note that in Protocol A $\alpha_1/\alpha_2 = 4/5$ while Protocol B $\alpha_1/\alpha_2 = 7/7$) (see dashed lines in Fig. 2a). Figure 2b shows the computed CNR between two tissues of successive T_1 values (spacing of 0.05 secs), as a function of T_1 for the different protocols. The CNR of the new sequence parameters for the range of T_1 values for which the optimization was performed (corresponds to the integral of the curves in Fig. 2b from 1.1 to 1.9 s) increased by 51%, which when taking into account the reduced number of excitations due to partial Fourier (PF) sampling ($CNR = CNR\sqrt{PF}$) is of $\sim 33\%$ (see Fig. 2b).

Figure 4 shows midbrain MP2RAGE and MP2RAGE_{WMGM} images. It is possible to see an increased delineation of the thalamus and its medio dorsal, ventral lateral and pulvinar nuclei (white arrows) as well as increase contrast within the brain stem (yellow arrows). It should be noted that the reduced intensity (darker MP2RAGE intensity) observed in cortical grey matter and deep brain structures does not reflect a reduction in SNR in those regions but simply the fact that the two images (GRE_{T11} and GRE_{T12}) have similar amplitudes but opposite phases (see Fig. 2a). Table 1 shows contrast to noise values (calculated as in Eq. 2) between different regions of interest: Medial Thalamus vs outer thalamus; outer thalamus vs WM; Caudate vs the head of the Putamen; Brain Stem vs cerebellum white matter; on average the increase of the contrast to noise ratio increased by 34%, in good agreement with what was expected from simulations. Naturally, the MIP and Full Range image have contrast to noise properties that, from a quantitative perspective, are equivalent to those of MP2RAGE_{WMGM}, (see Table 1). The main differences are the easier interpretability of the full range image (4th column of Fig. 4) due to its conventional appearance (dark CSF and bright WM), while the MIP image (3rd column of Fig. 4), having a similar appearance to Double Inversion recovery images naturally allow a tighter image display dynamic range.

Figure 5 shows lookup tables associated with different protocols (ii.a and ii.b, see Methods section for more details) for 3 different relative B_1^+ intensities (0.6, 1 and 1.4 times the nominal B_1). The

increased B_1^+ sensitivity of the protocol in Fig. 5a (ii.a) is related to the increase of the number of rf pulses used per GRE block and of their amplitude (one direct and one indirect consequence of increasing the spatial resolution of the T_1 maps and wanting to achieve optimum contrast). The protocol shown as insensitive to B_1^+ has errors on the T_1 estimation that are always lower than 2.5% of the nominal value (for the range of T_1 values expected to be found in the brain at 7T) even in the presence of $\pm 40\%$ deviations from the nominal B_1^+ (see Fig. 5d). Such low sensitivity to the B_1^+ inhomogeneity (before any B_1^+ correction) makes it a valuable protocol to validate the results achieved with the B_1^+ correction procedure.

Figure 6 shows different slices of R_1 maps of one subject (whose range $0.75\text{--}0.95 \text{ s}^{-1}$ was adapted to enhance the variations observed within white matter) obtained with two different imaging protocols and at two different head and dielectric pads [28,29] positions (in order to create different B_1 interference patterns). The B_1^+ maps, spatially co-registered to the R_1 maps, are also shown (Fig. 6d,h) in a short range of relative B_1 values (0.3–1.4). It is possible to see that the major changes between the two B_1 maps are located in the parietal and cerebellum regions. Red arrows show regions where the spatial inhomogeneities observed in the uncorrected R_1 maps (Fig. 6b,c) were spatially correlated with low B_1 regions (in the parietal area) or high relative B_1 (increased contrast observed in the splenium corpus callosum). After correction, the high resolution R_1 maps (Fig. 6f,g) have increased similarity to the low resolution R_1 maps (Fig. 6a,e), with a more homogeneous and symmetric distribution of R_1 values throughout the brain. Regions where the B_1 was too low to achieve the adiabatic condition in the bottom of the cerebellum (white arrow) cannot be corrected with the proposed methodology. Note that the low resolution R_1 maps (Protocol ii-B) remain mostly unchanged before (Fig. 6a) and after correction (Fig. 6e), supporting its insensitivity to B_1 inhomogeneities. Highly myelinated white matter fiber bundles such the optic radiation and the Genu corpus callosum are enhanced with respect to the remaining white matter (blue arrows) even after correction.

Figure 7 shows three different slices of R_1 maps of the human brain (the range, $0.45\text{--}0.80 \text{ s}^{-1}$, was set to enhance the variations observed within grey matter). In any of the R_1 maps it is possible to

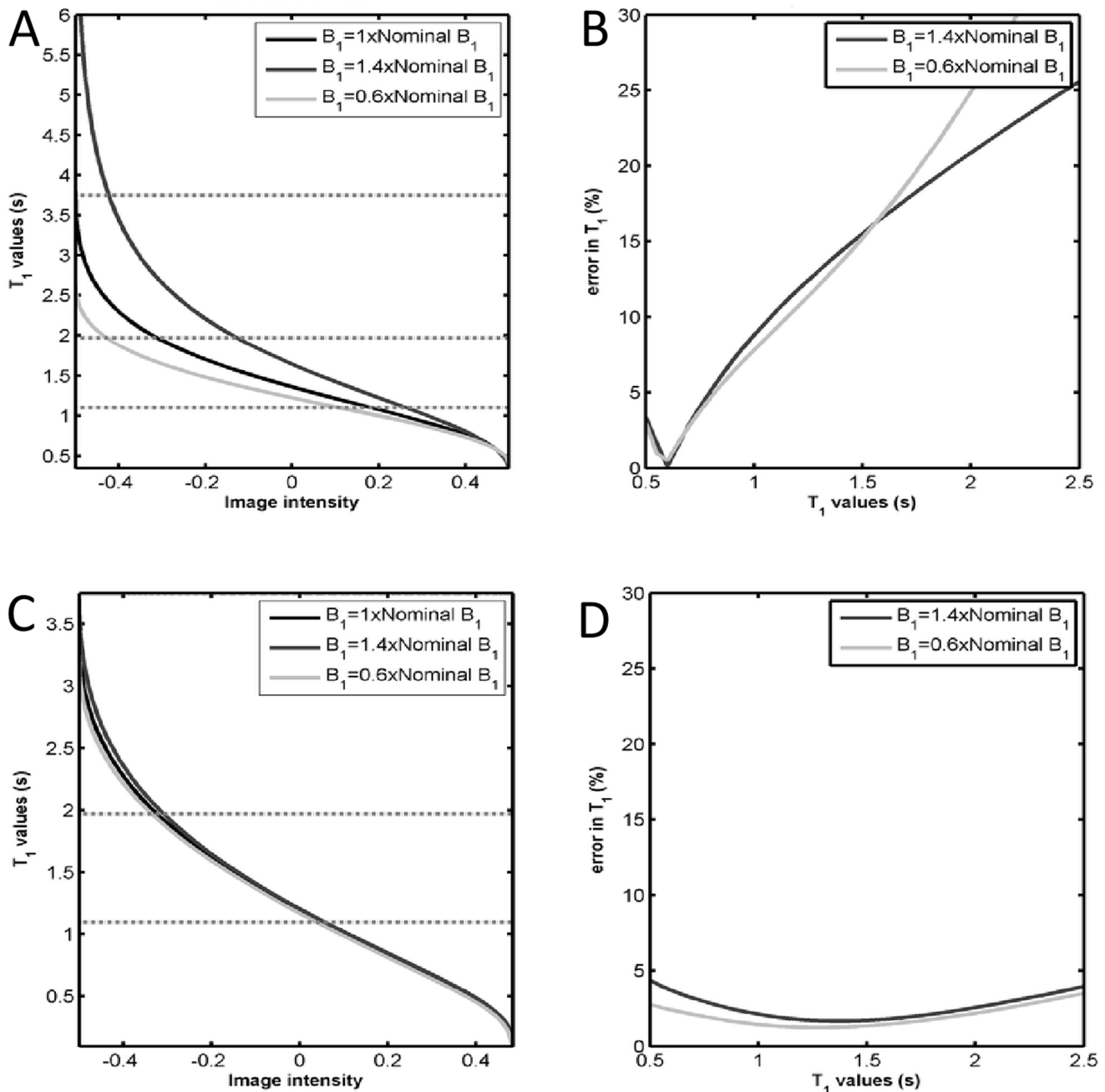


Figure 5. Plots of the look up tables (a,c) of the MP2RAGE intensity as a function of the T_1 values and the associated error (b,d) on the T_1 calculation as a function of T_1 when in the presence of B_1 values that are $\pm 40\%$ different from the nominal value (light and dark gray respectively). Protocols A and B are shown in the top (a,b) and bottom panel (c,d) respectively.
doi:10.1371/journal.pone.0069294.g005

observe the expected distribution of R_1 in the cortex with higher R_1 values being present on primary sensory areas (singled out by blue arrows), such as the sensory motor, auditory and visual cortex, with respect to other neighboring regions. Nevertheless, it is also possible to observe in Fig. 7b (uncorrected R_1 maps) that many cortical inhomogeneities/asymmetries are observed (as pointed out by the red arrows) that are likely to be associated with the B_1 inhomogeneity and are indeed removed when taking the B_1 measurements into account (Fig. 7c). Figure 7d shows the inflated right hemisphere of an high resolution corrected R_1 map of one single subject across the middle layer of the cortex. Blue

arrows show the same cortical regions as those shown on Figure 7c, with the primary sensory areas clearly having increased R_1 values when compared to the remaining cortex. Figure 8 shows an enlarged view of R_1 maps in the hippocampal region demonstrating that the high resolution of the obtained R_1 maps offers the possibility to use this quantitative information to visualize (the shape and separation between grey and white matter regions) and characterize its different fields and regions (with the dentate gyrus, DG, having the lowest R_1 values, followed by the CA1–CA3 and finally the CA4 and subiculum having higher R_1 values) [32]. The observation of the DG having a lower R_1 value than the CA fields

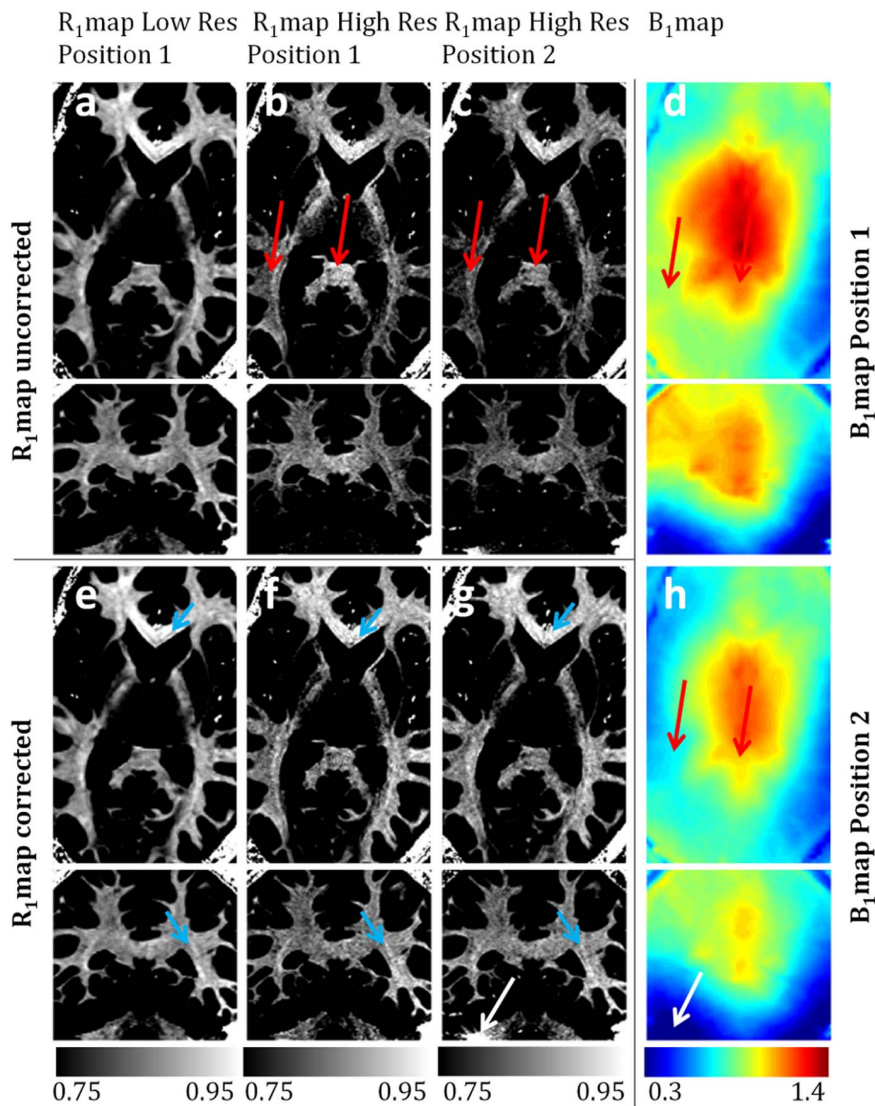


Figure 6. Transverse and coronal slices of: (a) Uncorrected R_1 maps using protocol ii-B; (b,c) Uncorrected R_1 maps using using protocol ii-A with two different head and dielectric pad positions; (e) Corrected R_1 maps using protocol ii-B; (f,g) Corrected R_1 maps using using protocol ii-A with two different head and dielectric pad positions; (e,h) B_1^+ maps corresponding to the two different head and dielectric pad positions; R_1 maps are shown in a short range from 0.75 to 0.95 s^{-1} to emphasize the sensitivity of the R_1 maps to the B_1 in-homogeneity, and the success of its correction. Arrows point out regions of increased difference between in the B_1^+ maps that have clear implications on the uncorrected high resolution R_1 maps. Blue arrows point out white matter fiber bundles with increased R_1 values with respect to the remaining white matter. Red arrows point out regions of significant R_1 differences from the ground truth prior to the B_1^+ correction, which are successfully corrected. The white arrow points out a region of very low B_1^+ field where the adiabatic condition was not reached and hence the R_1 values are largely overestimated and not possible to correct with the proposed methodology.
doi:10.1371/journal.pone.0069294.g006

is in good agreement with recent histology literature [33]. A clear delineation of all these structures is only discernible in the high resolution dataset and its relaxometry properties could show changes preceding the changes in volume often observed in pathologies.

Discussion

In this paper we have shown the ability to adapt the conventional T_1 weighted protocol used for whole brain imaging at 7T to focus on the tissues whose T_1 's lie in-between those of white and grey matter. Such adaptation allowed the visualization of thalamic nuclei and brain stem structures which were not visible in the conventional protocol because of lack of contrast to noise

ratio (note that the observed contrast is still only related to the T_1 of the different tissues). Particularly, the increased sensitivity to changes of grey and white matter T_1 values could help detect or/and characterize early stages of idiopathic Parkinson disease [34] that have been associated with deposition of Lewy bodies in the medulla oblongata and structural changes that progress in a caudorostral pattern [35,36], only affecting the substantia nigra in a stage where the first motor symptoms occur. Furthermore, the ability to recalculate a conventional T_1 -w contrast (where the contrast of subthalamic nuclei is still increased) could be used to obtain automatic segmentation of the whole brain, the thalamus and subsequently of its nuclei using available histology based atlas [37]. The better visualization or automatic delineation of some of

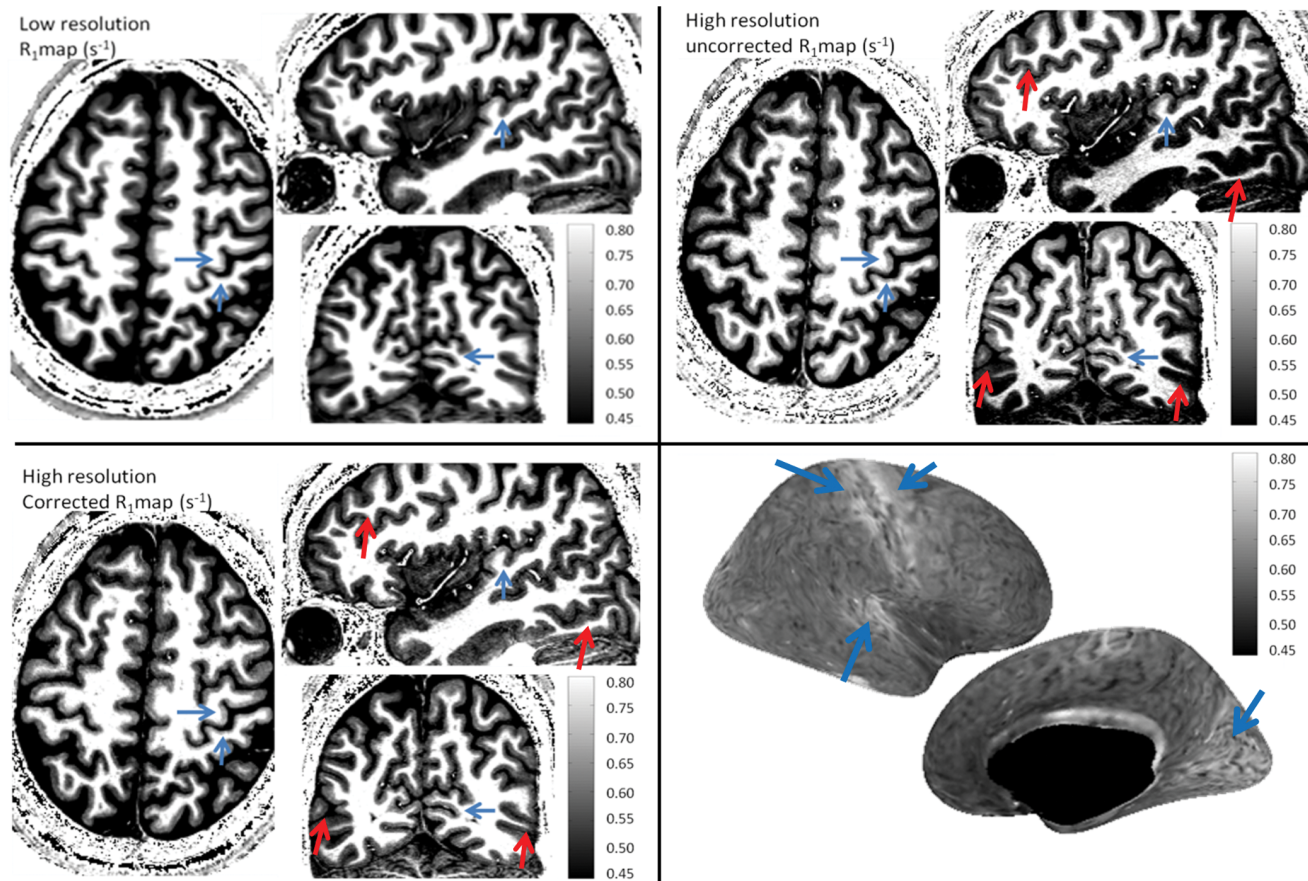


Figure 7. Transverse, sagittal and coronal slices of: (a) a corrected R_1 map using protocol B and (b,c) uncorrected and corrected R_1 maps calculated using protocol A. The R_1 maps are shown in a short range from 0.45 to 0.80 s^{-1} in order to emphasize the sensitivity of the cortical R_1 maps to the B_1 inhomogeneity. Panel (d) shows the reconstructed corrected R_1 surface across the middle layer of the cortex in the right hemisphere as calculated by freesurfer. Blue arrows point out primary sensory cortices (visual, auditory and sensory-motor cortex) which can be associated with increased R_1 values. Red arrows point out regions of significant R_1 differences from the ground truth prior to the B_1^+ correction, which are successfully corrected: on the coronal slice a strong left right asymmetry between similar cortical regions, while on the sagittal slice a strong anterior posterior variation is highlighted.

doi:10.1371/journal.pone.0069294.g007

these structures would allow a better localization of structures such as the vim [6] which is of great importance in pre-surgery planning in pathologies such as in Parkinson's disease or dystonia [8,9].

In this work, it was demonstrated that the residual sensitivity to B_1 inhomogeneities present in the R_1 maps obtained with the MP2RAGE sequence can be removed using information from a B_1 map (the choice of the B_1 mapping technique is not crucial, and many other methods would be equally valid). In its current implementation, the B_1 correction to the R_1 maps was only considered to affect the excitation pulses and not the adiabatic inversion pulse, this could be introduced into the Bloch equation simulations by changing the inversion efficiency of the inversion pulse as a function of B_1 and B_0 map. This would be expected to have only a small effect on the R_1 values measured as one of the main characteristics of the adiabatic pulse used is its low sensitivity to B_1 and B_0 variations once the adiabatic condition is achieved [38]. The success of the correction presented in this manuscript allows to obtain R_1 maps in either: a reduced acquisition time (decreasing TR will now only have implication in terms of available contrast to noise [5]); increase contrast to noise ratio thanks to the possibility of using protocols with increased flip angles; increased resolution thanks to the possibility of using longer

GRE blocks that would otherwise affect the B_1 insensitivity of the method.

High spatial resolution R_1 mapping at 3T has been shown to allow the identification of various cortical regions which have been validated by functional retinotopic and tonotopic studies [20,39]. The presented protocol to obtain quantitative R_1 values could be used in similar studies as there are remarkable similarities between the surface maps obtained (see Fig. 7d) with those found in literature, in which cortical regions were carefully validated with functional studies and the robustness of the methods were tested via test-retest of these regions in group studies. Although a comparison between the two methodologies is outside the scope of this paper (as the differences could result from the increased SNR, or R_1 dispersion available at 7T, or from the different efficiency of the R_1 mapping methodologies), it should be noted that the present study was acquired with a higher spatial resolution (0.65 mm vs 0.8 mm isotropic), was obtained in a shorter amount of time (12 mins vs 21 mins) and the through layer smoothing of the surface map shown on Fig. 7d was significantly smaller (2 mm vs 4 mm) than the cortical R_1 maps shown in previous studies [20,39]. Two considerations can be made from this observation: the proposed protocol has the potential to obtain a delineation of the primary sensory regions on individual subject data as shown by

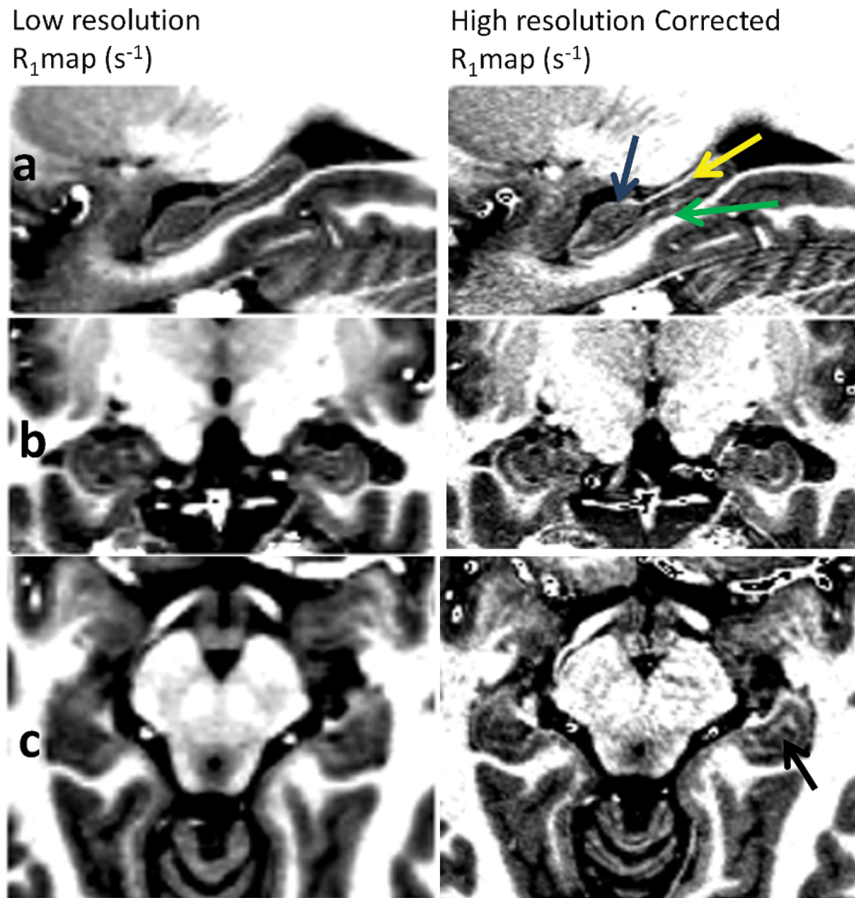


Figure 8. Transverse (a), sagittal (b) and coronal (c) slices covering the hippocampus of a high resolution corrected R_1 map. Arrows show hippocampal structures: CA1, CA2/3 (blue arrow); fimbria of hippocampus (yellow arrow); CA4 and DG (black arrow); subiculum (green arrow) [32]. Such structures are only discernible in the high resolution dataset.
doi:10.1371/journal.pone.0069294.g008

other groups; having a spatial resolution of the order of magnitude of the thickness of the different cortical layers (which have been demonstrated to have different relaxation properties) [7], makes the evaluation of R_1 maps at different cortical depths meaningful, such extra information could help further differentiating cortical regions [7,40] and will be the object of future research.

Future Work and Conclusions

We have shown that, by optimizing the contrast of the MP2RAGE sequence to a specific range of T_1 's at 7T, it is possible to gain access to clearer anatomical delineation of thalamic nuclei and brain stem structures. Such improved contrast could be an important asset in the context of automatic segmentation and in pre-surgical planning of Parkinson patients. One of the unanswered questions that will be the object of future work is the relationship between the observed sub-structures of the thalamus observed in T_1 -w imaging and the sub-thalamic nucleus identified with histology so that the automatic segmentation of the thalamus can be guided by the image contrast rather than simply the strength of the given prior.

References

1. Vaughan JT, Garwood M, Collins CM, Liu W, DelaBarre L, et al. (2001) 7T vs. 4T: RF power, homogeneity, and signal-to-noise comparison in head images. *Magn Reson Med* 46: 24–30.
2. Li TQ, van Gelderen P, Merkle H, Talagala L, Koretsky AP, et al. (2006) Extensive heterogeneity in white matter intensity in high-resolution T_2^* -weighted MRI of the human brain at 7.0 T. *NeuroImage* 32: 1032–1040.

We demonstrated the ability to obtain high resolution (0.65 mm isotropic) and high SNR R_1 maps of the whole brain in ~ 12 mins using the information from separately acquired R_1 and B_1 maps from the MP2RAGE and Sa2RAGE sequences. The quantitative R_1 maps revealed subtle differences between distal GM tissues as shown in previous studies, but also within WM where R_1 contrast is usually overlooked.

Acknowledgments

The authors would like to thank Dr. Tobias Kober for the support in the implementation and maintenance of the sequences used throughout this study and Dr. Kieran O'Brien for having built the dielectric pads used to accentuate the B_1 field variations in the scan-rescan experiment.

Author Contributions

Conceived and designed the experiments: JPM RG. Performed the experiments: JPM. Analyzed the data: JPM. Contributed reagents/materials/analysis tools: RG. Wrote the paper: JPM.

3. Duyn JH, Van Gelderen P, Li TQ, De Zwart JA, Koretsky AP, et al. (2007) High-field MRI of brain cortical substructure based on signal phase. *Proceedings of the National Academy of Sciences of the United States of America* 104: 11796–11801.
4. Van de Moortele PF, Auerbach EJ, Olman C, Yacoub E, Ugurbil K, et al. (2009) T(1) weighted brain images at 7 Tesla unbiased for Proton Density, T(2) contrast and RF coil receive B(1) sensitivity with simultaneous vessel visualization. *Neuroimage*.
5. Marques JP, Kober T, Krueger G, van der Zwaag W, Van de Moortele PF, et al. (2010) MP2RAGE, a self bias-field corrected sequence for improved segmentation and T-1-mapping at high field. *Neuroimage* 49: 1271–1281.
6. Friehs GM, Park MC, Goldman MA, Zerris VA, Noren G, et al. (2007) Stereotactic radiosurgery for functional disorders. *Neurosurg Focus* 23: E3.
7. Geyer S, Weiss M, Reimann K, Lohmann G, Turner R (2011) Microstructural Parcellation of the Human Cerebral Cortex - From Brodmann's Post-Mortem Map to in vivo Mapping with High-Field Magnetic Resonance Imaging. *Front Hum Neurosci* 5: 19.
8. Pinski MO, Volkmann J, Falk D, Herzog J, Steigerwald F, et al. (2009) Deep brain stimulation of the internal globus pallidus in dystonia: target localisation under general anaesthesia. *Acta Neurochir (Wien)* 151: 751–758.
9. Pinski MO, Volkmann J, Falk D, Herzog J, Alfke K, et al. (2008) Electrode implantation for deep brain stimulation in dystonia: a fast spin-echo inversion-recovery sequence technique for direct stereotactic targeting of the GPI. *Zentralbl Neurochir* 69: 71–75.
10. Traynor CR, Barker GJ, Crum WR, Williams SC, Richardson MP (2011) Segmentation of the thalamus in MRI based on T1 and T2. *Neuroimage* 56: 939–950.
11. Deoni SC, Rutt BK, Parrent AG, Peters TM (2007) Segmentation of thalamic nuclei using a modified k-means clustering algorithm and high-resolution quantitative magnetic resonance imaging at 1.5 T. *Neuroimage* 34: 117–126.
12. Behrens TE, Johansen-Berg H, Woolrich MW, Smith SM, Wheeler-Kingshott CA, et al. (2003) Non-invasive mapping of connections between human thalamus and cortex using diffusion imaging. *Nat Neurosci* 6: 750–757.
13. Abosch A, Yacoub E, Ugurbil K, Harel N (2010) An assessment of current brain targets for deep brain stimulation surgery with susceptibility-weighted imaging at 7 tesla. *Neurosurgery* 67: 1745–1756; discussion 1756.
14. Helms G, Draganski B, Frackowiak R, Ashburner J, Weiskopf N (2009) Improved segmentation of deep brain grey matter structures using magnetization transfer (MT) parameter maps. *Neuroimage* 47: 194–198.
15. Baudrexel S, Nurnberger L, Rub U, Seifried C, Klein JC, et al. (2010) Quantitative mapping of T1 and T2* discloses nigral and brainstem pathology in early Parkinson's disease. *Neuroimage* 51: 512–520.
16. Sudhyadhom A, Haq IU, Foote KD, Okun MS, Bova FJ (2009) A high resolution and high contrast MRI for differentiation of subcortical structures for DBS targeting: the Fast Gray Matter Acquisition T1 Inversion Recovery (FGATIR). *Neuroimage* 47 Suppl 2: T44–52.
17. Cho ZH, Son YD, Kim HK, Kim NB, Choi EJ, et al. (2011) Observation of glucose metabolism in the thalamic nuclei by fusion PET/MRI. *J Nucl Med* 52: 401–404.
18. Tanner M, Gambarota G, Kober T, Krueger G, Erritzoe D, et al. (2012) Fluid and white matter suppression with the MP2RAGE sequence. *J Magn Reson Imaging* 35: 1063–1070.
19. Glasser MF, Van Essen DC (2011) Mapping human cortical areas in vivo based on myelin content as revealed by T1- and T2-weighted MRI. *J Neurosci* 31: 11597–11616.
20. Sereno MI, Lutti A, Weiskopf N, Dick F Mapping the Human Cortical Surface by Combining Quantitative T1 with Retinotopy. *Cereb Cortex*.
21. Fleysher R, Fleysher L, Liu S, Gonen O (2008) TriTone: a radiofrequency field (B1)-insensitive T1 estimator for MRI at high magnetic fields. *Magn Reson Imaging* 26: 781–789.
22. Hsu JJ, Zaharchuk G, Glover GH (2009) Rapid methods for concurrent measurement of the RF-pulse flip angle and the longitudinal relaxation time. *Magn Reson Med* 61: 1319–1325.
23. Deichmann R (2005) Fast high-resolution T1 mapping of the human brain. *Magn Reson Med* 54: 20–27.
24. Deoni SC (2011) Correction of main and transmit magnetic field (B0 and B1) inhomogeneity effects in multicomponent-driven equilibrium single-pulse observation of T1 and T2. *Magn Reson Med* 65: 1021–1035.
25. Preibisch C, Deichmann R (2009) Influence of RF spoiling on the stability and accuracy of T1 mapping based on spoiled FLASH with varying flip angles. *Magn Reson Med* 61: 125–135.
26. Yarnykh VL (2010) Optimal radiofrequency and gradient spoiling for improved accuracy of T1 and B1 measurements using fast steady-state techniques. *Magn Reson Med* 63: 1610–1626.
27. Eggenschwiler F, Kober T, Magill AW, Gruetter R, Marques JP (2012) SA2RAGE: A new sequence for fast B(1) (+) -mapping. *Magn Reson Med* 67: 1609–1619.
28. Teeuwisse WM, Brink WM, Haines KN, Webb AG (2012) Simulations of high permittivity materials for 7 T neuroimaging and evaluation of a new barium titanate-based dielectric. *Magn Reson Med* 67: 912–918.
29. Teeuwisse WM, Brink WM, Webb AG (2012) Quantitative assessment of the effects of high-permittivity pads in 7 Tesla MRI of the brain. *Magn Reson Med* 67: 1285–1293.
30. Rorden C, Brett M (2000) Stereotaxic display of brain lesions. *Behav Neurol* 12: 191–200.
31. Fischl B, Salat DH, van der Kouwe AJ, Makris N, Segonne F, et al. (2004) Sequence-independent segmentation of magnetic resonance images. *Neuroimage* 23 Suppl 1: S69–84.
32. Van Leemput K, Bakour A, Benner T, Wiggins G, Wald LL, et al. (2009) Automated segmentation of hippocampal subfields from ultra-high resolution in vivo MRI. *Hippocampus* 19: 549–557.
33. Abraham H, Vincze A, Veszpremi B, Kravjak A, Gomori E, et al. (2012) Impaired myelination of the human hippocampal formation in Down syndrome. *Int J Dev Neurosci* 30: 147–158.
34. Jubault T, Brambati SM, Degroot C, Kullmann B, Strafella AP, et al. (2009) Regional Brain Stem Atrophy in Idiopathic Parkinson's Disease Detected by Anatomical MRI. *Plos One* 4.
35. Braak H, Del Tredici K (2004) Alzheimer's disease: intraneuronal alterations precede insoluble amyloid-beta formation. *Neurobiol Aging* 25: 713–718; discussion 743–716.
36. Braak H, Del Tredici K (2004) Poor and protracted myelination as a contributory factor to neurodegenerative disorders. *Neurobiol Aging* 25: 19–23.
37. Krauth A, Blanc R, Poveda A, Jeanmonod D, Morel A, et al. (2010) A mean three-dimensional atlas of the human thalamus: generation from multiple histological data. *Neuroimage* 49: 2053–2062.
38. Hurley AC, Al-Radaideh A, Bai L, Aickelin U, Coxon R, et al. (2010) Tailored RF pulse for magnetization inversion at ultrahigh field. *Magn Reson Med* 63: 51–58.
39. Dick F, Taylor Tierney A, Lutti A, Josephs O, Sereno MI, et al. (2012) In vivo functional and myeloarchitectonic mapping of human primary auditory areas. *J Neurosci* 32: 16095–16105.
40. Marques JP, Gruetter R. Exploring cortical cytoarchitecture in high resolution R1 maps; 2013; Salt Lake City, UT, USA. Proceedings of the 21st ISMRM Annual Meeting.